An Energy-Saving Solution for Hydrogen Conductivity Measurement Systems in Thermal Power Plant Boiler Water Based on Deep Regeneration Technology Using Ion-Exchange Resins

Tianbo Ma[1], Le Chen[1*], Heng Jiang[1], Yachao Li[1], Xuebin Yang[1], Honglei Cui[1], Jun Zhang[1]
[1]Department of State Grid–Energy Hami Coal & Power Co., Ltd., Huayuan Power Plant, Hami 839000, Xinjiang, China
Corresponding author: Le Chen (e-mail: 13955416142@163.com).

ABSTRACT To address discontinuous boiler water hydrogen conductivity measurement, low resin exchange output, high plant energy consumption, and frequent offline regeneration of resin columns in thermal power plants, an accuracy-constrained energy consumption optimization model for deep regeneration of ion exchange resins was developed. Based on the traditional hydrogen-type cation exchange resin column measurement process, the model integrates hydrogen generation through ionization, ion migration, online resin reset, and four-channel independent regeneration control, forming a closed-loop framework of "capacity identification—trend determination—liquid volume and time optimization—accuracy-constrained control." Real-time parameters, including flow rate, pressure, temperature, hydrogen conductivity, regeneration voltage, and current, are collected to identify resin exchange-capacity decay, determine regeneration timing and triggering conditions, and optimize regeneration power and cycle duration. The optimization is constrained by a measurement error of $\leq 3\%$ and a cation removal efficiency of $\geq 99.9\%$. A 30-day test on Huayuan Unit 1 and Unit 3 at 20 test points showed that the average effective resin exchange quantity increased from 0.97 $mmol{\cdot}mL^{-1}$ to 1.50 $mmol{\cdot}mL^{-1}$, the average failure interval extended from 7.7 days to 29.3 days, and total system energy consumption decreased from 173.4 kWh to 112.5 kWh, representing a 35.12% reduction. After deep regeneration, the average relative error decreased to 1.14%, and the effective data rate increased to 99.36%. These results indicate that the model reduces regeneration and maintenance energy consumption while ensuring the accuracy of boiler water hydrogen conductivity measurement.

INDEX TERMS ion exchange resin; deep regeneration; reactor water hydrogen conductivity; energy consumption optimization; thermal power plant

I. INTRODUCTION

Ion exchange resins have become essential materials in the fields of water treatment, ion separation, and pollutant reduction. Over the past three years, international research has shifted from evaluating adsorption capacity alone to the synergistic optimization of regeneration efficiency, operational lifespan, and online monitoring. Godifredo et al. (2024) utilized natural zeolite ion exchange columns for nitrogen recovery from the permeate of an anaerobic membrane bioreactor, demonstrating that the ion exchange process can simultaneously serve the purposes of pollutant removal and resource recovery [1]; Yeoh et al. (2026) optimized the resin regeneration process by adjusting parameters such as pretreatment temperature, brine concentration, and resin-to-brine ratio, demonstrating that regeneration conditions directly affect resin lifespan, chemical consumption, and waste liquid load [2]; Marin et al. (2024) systematically reviewed the development trends of polymer ion exchange resins in wastewater treatment, pointing out that material modification and application-specific adaptation remain key to enhancing the stability of engineering applications [3]. Meanwhile, Wullenweber et al. (2024) focused on the adsorption and regeneration behavior of macroporous ion-exchange membrane adsorbers toward natural organic compounds [4], while Bernardi et al. (2024) utilized benchtop nuclear magnetic resonance (NMR) technology to track the Ni^{2+} removal process [5]. Existing research has advanced the development of resin materials, regeneration processes, and process characterization; however, most studies have focused on wastewater purification or heavy metal removal, with insufficient attention paid to the requirements for continuous regeneration, low-energy operation, and measurement accuracy in the context of online hydrogen conductivity (HC) monitoring of boiler water in thermal power plants. Hydrogen conductivity measurement systems have long been used for early warning of water and steam quality in thermal power plants boiler water. Traditional resin columns have offline regeneration, manual replacement, and bypass flushing which can cause problems with short regeneration times, frequent maintenance, high energy usage in flushing, and measurement lag. To solve these problems, this paper focuses on the deep regeneration technology of the ion-exchange resins, and combines the detection of resin capacity decay, hydrogen conductivity trend analysis, optimization of regeneration solution volume and regeneration cycle time and energy consumption control with the measurement accuracy limitation into an integrated algorithmic system to establish an online regeneration process: “sample water pretreatment—ionization to generate hydrogen—regeneration of resins—ion migration—continuous reset”. The 20 online hydrogen conductivity measurement points of Units 1 and 3 in Huayuan Power Plant were used to conduct the experiment, and it was found that after deep regeneration, the resin’s average effective exchange capacity increased from 0.97 mmol·mL^{-1} to 1.50 mmol·mL^{-1}, the total energy consumption of 30 days was reduced from 173.4 kWh to 112.5 kWh, and the average failure cycle was extended from 7.7 days to 29.3 days. This method saved energy and reduced consumption, and its average relative error was 1.14%, the effective data rate was 99.36%, which had engineering significance in synergistically optimizing the deep regeneration of resin online and monitoring the water and steam system of thermal power plant.

II. ANALYSIS OF THE BOILER WATER HYDROGEN CONDUCTIVITY MEASUREMENT SYSTEM AND ENERGY CONSUMPTION COMPOSITION IN THERMAL POWER PLANTS

The water conductivity measuring system of boiler water is composed of three parts: pretreating, cation exchange, conductivity detecting, and data collecting and controlling terminal. It is mainly used in the transport of sample water, the regeneration of resin, the direct current drive, and the on-line communication. The system is powered by 220 V AC $\pm$ 22 V; the regeneration voltage ranges from 5 to 24 V; the flow detection signal is 4 – 20 mA, corresponding to a sample water flow rate of 100 – 300 mL/min; Pressure exceeding 0.25 MPa triggers overpressure protection [6]. The controller collects, through an RTU-485 interface, flow, pressure, voltage, current, and hydrogen conductivity, and performs threshold assessment, fault coding, and operation state logging. The configuration of the system is illustrated in Figure 1, in order to clarify the energy transfer and information exchange between the functional units.

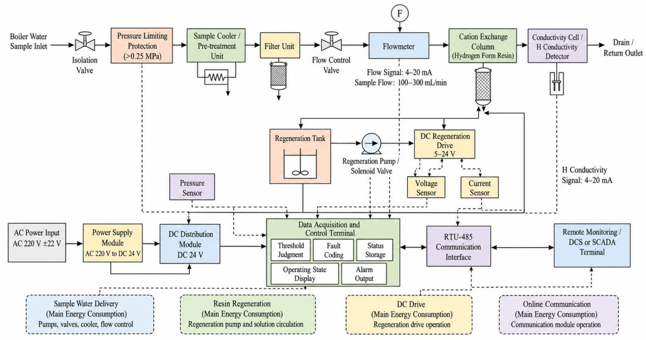

FIGURE 1. System Configuration Diagram of the Boiler Water Hydrogen Conductivity Measurement System for Thermal Power Plants.

III. DESIGN OF AN ENERGY-SAVING SOLUTION FOR THE BOILER WATER HYDROGEN CONDUCTIVITY MEASUREMENT SYSTEM IN THERMAL POWER PLANTS BASED ON DEEP REGENERATION USING ION-EXCHANGE RESIN

A. DESIGN OF THE DEEP REGENERATION PROCESS FLOW

Deep regeneration is carried out in accordance with the sequence of "Sample Water Pretreatment — Ionization to Generate Hydrogen — Resin Exchange — Ion Transfer — Successive Reset." After two stages of filtration, the sample water enters the regeneration module at a flow rate of 100 – 300 mL/min, with the inlet pressure controlled within 0.25 MPa; A 220 V AC $\pm$ 22 V power supply is rectified to output a 5 – 24 V DC voltage, causing the water to dissociate into H (and OH). Due to the selective effect of the cation exchange membrane, H ions are introduced into the resin chamber, and the cations, such as NH, NO, NO, NO, NO, are absorbed by the resin. The displaced ions are driven through the membrane and discharged by an electric field, while the resin simultaneously reverts to its H-type state [7]. The controller obtains 4 – 20 mA flow signals, as well as voltage, current, pressure, and hydrogen conductivity data. Through RTU-485, it uploads operational parameters to the four separate channels, and adjusts the operation frequency of the four separate channels according to flow, pressure, and regeneration load, simultaneously triggering the water cutoff, the power cut, and the over-pressure protection. In order to clarify the coupling of mass flow, ion flow, and control flow, Figure 2 shows a deep regeneration process.

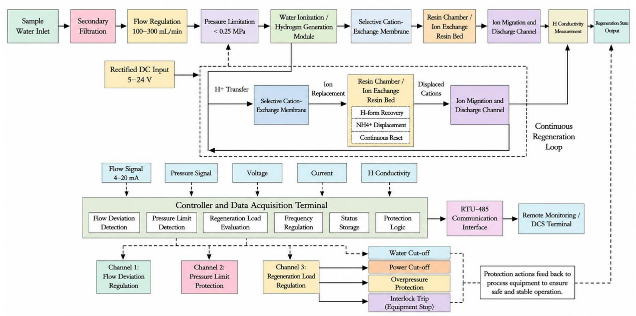

FIGURE 2. Process and Control Flowchart for Deep Regeneration of Ion Exchange Resin.

B. OPTIMIZATION OF RESIN EXCHANGE COLUMN STRUCTURE AND REGENERATION CIRCUIT

The resin exchange tower adopts a modular, segmented structure which integrates the sample water path, the H type strong acid cation exchange resin bed, the ion exchange membrane, and the regeneration electrode circuit. Four separate channels are arranged in parallel for power supply to avoid local over-regeneration due to continuous high load on one channel. The total feed rate is 100 – 300 mL/min, with a flow warning range of 10 – 300 mL/min. The AC 220 V $\pm$ 22 V power supply is rectified to output a DC voltage of 5 – 24 V. The AC 220 V $\pm$ 22 V power supply is rectified to output a DC voltage of 5 – 24 V. When the inlet water pressure is greater than 0.25 MPa, the regeneration output is stopped when the water pressure is greater than 0.25 MPa, and the regeneration output is stopped when water or electricity is cut off [8]. The energy consumption per unit of sample water during regeneration is defined as:

$$e_r = \frac{\sum_{k=1}^{4} U_k I_k}{Q}. \tag{1}$$

where e_r represents the specific energy consumption per regeneration, U_k and I_k are the regeneration voltage and current for the k-th channel, respectively, Q is the total sample water flow rate through the exchange column, and k is the channel number. The RTU-485 terminal at the same time records the flow, pressure, and electric parameters to determine the range of operation under low pressure and low power consumption; the constraint relation is shown in Figure 3.

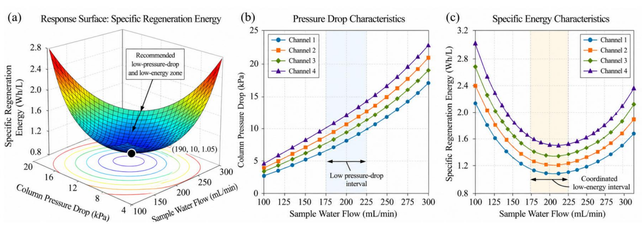

FIGURE 3. Optimization Curves for Sample Water Flow Rate, Exchange Column Pressure Drop, and Regeneration Specific Energy Consumption.

C. COORDINATED CONTROL SCHEME FOR MEASUREMENT, REGENERATION, AND BYPASS SWITCHING

In order to ensure continuity in the measurement of hydrogen conductivity and to reduce the energy consumption caused by unnecessary regeneration, a three level coordinated control strategy is implemented based on the measurement state, regeneration load, and equipment availability. The concrete scheme is as follows:

(1) Measurement Control: The sample water is fed into the ion generator through a two-stage filtering system; the purified water is fed to the conductive electrode, and the waste water is discharged into the drain groove. Flow, pressure, hydrogen conductivity, and the state of the device are continuously monitored by the controller. As soon as the parameters have stabilised, the recording of the measurement data is enabled; in the event of abnormal conditions, the validity flag shall be frozen so as not to affect the evaluation of the water quality.

(2) Regeneration Control: the four regeneration passages are started and stopped independently according to the water load of the sample. Long term full-power operation is inhibited by rotation activation and frequency adjustment. Once the water supply is interrupted, the power is lost, or the pressure is greater than 0.25 MPa, the regeneration circuit is shut down immediately and a fault code is generated.

(3) Bypass Switching: If the device fails or during the start-up phase of the unit, the system is switched to a backup resin column, with 1-2 regenerated resin columns remaining active on site. After startup, the system operates in bypass mode for 6 – 12 hours. Once the specific conductivity of the sample water falls below 15 μS/cm, the controller checks the position of the valve, the flow and the pressure state prior to switching to the smart ion generator measuring circuit [9].

D. LOW-ENERGY CONSUMPTION OPERATION MODE AND SYSTEM SAFETY PROTECTION DESIGN

Low-energy operation is based on a combined control strategy consisting of a state machine and multi-constraint optimization which is based on the coordinated switching mechanism. Depending on the sample water load, the controller alternates between 4 modes: Standby, Economy, Adaptive and Protective Bypass. The controller optimises the flow rate by varying the start/stop combination and frequencies of the four separate regeneration channels, which ensures that the regeneration output is adjusted to the flow rate and the ion-exchange load is not operated at full power for a long time. It can be operated in the temperature range of 0–40 °C, the range of regeneration voltage is 5–24 V, and the feedback signal is 4–20 mA, corresponding to the sample water flow rate of 100–300 mL/min. When the pressure is over 0.25 MPa, the flow is not in the range of 10-300 mL/min or the water supply is cut off, or the power is out, the system cuts off the output of regeneration and generates the fault code [10]. If the specific conductivity of the sample water has not reached the target value below 15 μS/cm after 6–

12 hours from the start up of the unit, the bypass to the standby resin column is kept. The RTU-485 is continually uploading voltage, current, flow rate, pressure and interlock status, etc., while also including safety constraints in energy consumption optimization. In Table 1 some operating modes and protective actions are indicated. The complete control goal for one cycle of the system is stated as:

$$J_t = \alpha \frac{\sum_{k=1}^{4} U_{k,t} I_{k,t} s_{k,t}}{Q_t} + \beta \left(\frac{Q_t - Q_s}{Q_s} \right)^2 + \gamma \sum_{j=1}^{3} [\max(0, g_{j,t})]^2 . \quad (2)$$

Where, J_t is the comprehensive cost for the t-th control cycle; $U_{k,t}$ and $I_{k,t}$ are the voltage and current of the k-th regeneration channel, respectively; $s_{k,t}$ is the channel start/stop variable, set to 1 when active and 0 when inactive; Q_t is the actual sample water flow rate; Q_s is the setpoint flow rate; $g_{j,t}$ is the exceedance limit for the three types of constraints: overpressure, low flow, and high flow; α, β, and γ are the weighting coefficients for regeneration energy consumption, flow deviation, and safety risk, respectively.

TABLE 1. Low-Energy Consumption Operating Mode and System Safety Protection Strategy

Operating Mode	Entry Conditions	Regeneration and Measurement Control	Safety Protection Actions
Standby Mode	No valid sample water or system in initialization	All 4 regeneration channels are disabled; only state parameter acquisition and communication are maintained	DC output is disabled; device status is preserved
Economy Mode	Flow rate is between 100 and 300 mL/min and parameters are within limits	Engages the minimum number of channels based on exchange load; voltage is automatically adjusted within the 5–24 V range	Continuously monitors pressure, flow, and power supply status
Adaptive Mode	Changes in sample flow rate or ion exchange load	Adjusts valve position, number of channels, and operating frequency based on 4–20 mA feedback	Diagnoses and issues early warnings regarding deviation trends
Protection Bypass Mode	Pressure $>$ 0.25 MPa, flow rate exceeds 10–300 mL/min, water supply interruption, or power failure	Stop regeneration and valid data output; switch to the standby resin column	Trigger pressure limit, circuit break, and fault alarms, and record status

IV. KEY ALGORITHMS FOR ENERGY-SAVING CONTROL IN BOILER WATER HYDROGEN CONDUCTIVITY MEASUREMENT SYSTEMS FOR THERMAL POWER PLANTS

A. ALGORITHM FOR IDENTIFYING RESIN EXCHANGE CAPACITY DECLINE

The method of identifying the degradation of resin exchange capacity is implemented in the following order: data verification, load integration, capacity estimation, and trend analys. The controller obtains the original water conductivity, the hydrogen conductivity, the temperature, the pressure and the four regeneration current channels through RTU-485, and converts the 4 – 20 mA signal into engineering variables; when the pressure is greater than 0.25 MPa, or when the water is cut or the power is cut off, the data point is recorded only as the fault flag and is not included in the model update [11]. Taking into account the fact that the cation adsorption and the electric regeneration compensation take place at the same time, the residual exchange capacity is defined as:

$$\hat{C}_t = C_0 - \sum_{i=1}^{t} Q_i \hat{c}_i \Delta t + \frac{\eta_F}{F} \sum_{i=1}^{t} \sum_{k=1}^{4} s_{k,i} I_{k,i} \Delta t. \quad (3)$$

where $\hat{C}_t$ and C_0 represent the current estimated capacity and initial effective capacity, respectively; Q_i is the sample water flow rate; $\hat{c}_i$ is the equivalent cation concentration inverted based on the compensation relationships between the two types of conductivity and temperature; Δt is the sampling interval; η_F is the charge utilization coefficient; F is Faraday's constant; and $s_{k,i}$ and $I_{k,i}$ are the on/off variables and regeneration current for channel k, respectively. To suppress sudden changes in capacity estimates caused by operating conditions, a recursive smoothing method is used to construct the health index:

$$H_t = \lambda H_{t-1} + (1 - \lambda) \frac{\hat{C}_t}{C_0}. \quad (4)$$

where H_t is the capacity health index, and λ is the historical information forgetting factor. Persistent degradation is identified using one-sided cumulative deviation:

$$G_t = \max\left[0, G_{t-1} + H_{\text{ref}} - H_t - \delta\right]. \quad (5)$$

where G_t is the cumulative decay amount, H_{ref} is the baseline health level, and δ is the allowable fluctuation band. When G_t exceeds the set threshold and the cation removal rate approaches the control boundary of 99.9%, the algorithm outputs a capacity warning, decay level, and channel load status; it does not increase the regeneration power directly, but rather passes the recognition result to the following regeneration timing determining algorithm to prevent a continuous increase of 5 – 24 V regeneration voltage from masking irreversible resin aging [12].

B. REGENERATION TIMING DETERMINATION ALGORITHM BASED ON HYDROGEN CONDUCTANCE TRENDS

The regeneration timing determination algorithm is based on the continuous hydrogen conductivity sequence as the key input, and integrates the HMI output from sectio. It performs on-line calculations in accordance with the procedure of "Data Filtering — Temperature Correction — Trend Extraction — Area Accumulation — Trigger Decision".

The effective window is updated only when the inlet water pressure is between 0.15 and 0.20 MPa and the input water specific conductivity is less than 15 μS/cm. Data in excess of 0.25 MPa, water supply interruption, or loss of power are written into the anomaly queue and excluded from the trend fitting [13]. The temperature correction model for hydrogen conductivity is:

$$\kappa_t^{25} = \frac{\kappa_t}{1 + \alpha_T (T_t - 25)}. \tag{6}$$

where κ_t^{25} is the hydrogen conductivity converted to 25 °C, κ_t is the measured value at time step t, T_t is the sample water temperature, and α_T is the temperature compensation coefficient. The rate of change is calculated using exponential-weighted local regression:

$$b_t = \frac{\sum_{i=0}^{N-1} \rho^i (i - \bar{i})(\kappa_{t-i}^{25} - \bar{\kappa}_t)}{\sum_{i=0}^{N-1} \rho^i (i - \bar{i})^2}. \tag{7}$$

where b_t is the trend slope, N is the sliding window length, ρ is the historical data decay factor, and $\bar{i}$ and $\bar{\kappa}_t$ are the weighted time mean and weighted hydrogen conductivity mean, respectively. To prevent transient spikes from triggering unnecessary regeneration, the area of sustained exceedance is calculated as follows:

$$A_t = \sum_{i=0}^{N-1} \max(0, \kappa_{t-i}^{25} - \kappa_{\mathrm{ref}}) \Delta t. \tag{8}$$

where A_t is the cumulative excess area within the window, κ_{ref} is the steady-state reference value, and Δt is the sampling period. The comprehensive regeneration criterion is defined as:

$$D_t = w_1 \frac{b_t}{\theta_b} + w_1 \frac{A_t}{\theta_A} + w_3 (1 - H_t). \tag{9}$$

where D_t is the regeneration trigger index, H_t is the capacity health index, w_1, w_1, and w_3 are the weighting factors for slope, area, and capacity decay, and θ_b and θ_A are the corresponding normalized thresholds. When D_t continuously exceeds the trigger threshold, and the comparison error between the standard resin columns in parallel is within ± 3%, the controller generates a tiered regeneration command based on the load of each separate channel, and restricts the regeneration strength in accordance with the cation removal control objective. Then, the determination criteria are transferred to an algorithm for optimizing the consumption of the regeneration solution and the cycle time [14]. The increase of the hydrogen conductivity, the accumulated area, and the regeneration activation range are shown in Figure 4.

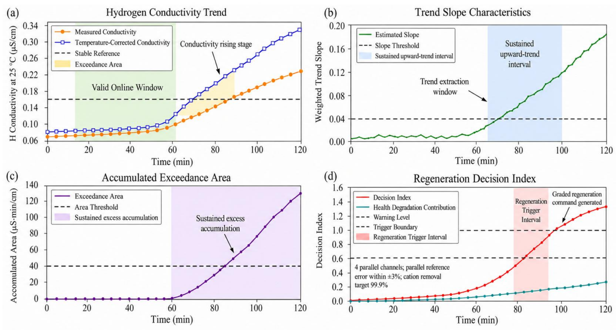

FIGURE 4. Hydrogen Conductivity Trend, Cumulative Area Exceeding the Threshold, and Regeneration Trigger Interval.

C. OPTIMIZATION ALGORITHM FOR REGENERATION SOLUTION CONSUMPTION AND CYCLE TIME

Due to the fact that the electrogeneration process does not contain the measuring step of hydrochloric acid, the algorithm defines the "regeneration solution consumption" as the volume of the electrogenerating solution that passes through the resin chamber, the membrane chamber, and the discharge branch in one control cycle, and then optimizes this by combining the cycle time, channel configuration, and DC power. The control program receives the output regeneration trigger index, reads the temperature, the pressure, the hydrogen conductivity, the state of the four channels, and the 4 – 20 mA feedback signal, constructs the candidate control vector, and carries out the rolling optimization under the constraints of the ambient temperature of 0 – 40 ° C, regeneration voltage 5 – 24 V, a pressure not exceeding 0.25 MPa, and a regeneration degree greater than 99.9%[15-16]. The complex objective function is designed as follows:

$$\min_{z_t} J_t = \alpha \frac{V_t}{V_b} + \beta \frac{\tau_t}{\tau_b} + \gamma \frac{\sum_{k=1}^{4} U_{k,t} I_{k,t} s_{k,t} \tau_t}{E_b} + \xi (1 - \hat{\eta}_t)^2. \tag{10}$$

In the equation, z_t is the decision vector for the t-th cycle; V_t is the regenerated liquid volume; τ_t is the cycle time; V_b, τ_b, and E_b are the normalization benchmarks for volume, time, and energy consumption, respectively; $U_{k,t}$, $I_{k,t}$, and $s_{k,t}$ are the voltage, current, and on/off variables for the k-th channel, respectively; $\hat{\eta}_t$ is the predicted regeneration degree; and α, β, γ, and ξ are the weighting factors for liquid volume, time, energy consumption, and regeneration quality. The regeneration degree is predicted using a coupled model of electric field strength, circulating liquid volume, and residence time:

$$\hat{\eta}_t = 1 - \exp\left[-K(T_t) V_t^{\mu} \tau_t^{\nu} \sum_{k=1}^{4} f_{k,t} s_{k,t} \right]. \tag{11}$$

where $K(T_t)$ is the temperature-dependent mass transfer coefficient, T_t is the liquid temperature, $f_{k,t}$ is the operating frequency of channel k, and μ and ν are the online-identified liquid volume and time response indices. The algorithm filters out samples involving water supply interruption, power failure, overpressure, and communication anomalies. It sorts feasible solutions in ascending order by J_t and outputs the setpoints for regeneration liquid volume, circulation time, and channel frequency[17]; the data boundaries are shown in Table 2.

TABLE 2. Input Parameters for Optimizing Regeneration Liquid Volume and Cycle Time

Parameter Category	Optimization Variables or Monitored Quantities	Design Boundaries	Algorithm Function
Regeneration Channel	$s_{k,t}, f_{k,t}$	4 independent channels	Generation channels start/stop and frequency modulation combination
Regenerative Voltage	$U_{k,t}$	DC 5–24 V	Constrained electric field drive force and power consumption
Signal Input	I_t	4–20 mA	Conversion of equipment operating feedback signals
Ambient temperature	T_t	0–40 °C	Corrected mass transfer coefficient
Pressure conditions	P_t	≤ 0.25 MPa	Terminate the current optimization cycle when limits are exceeded
Inlet water conditions	κ_{in}	< 12 μS/cm	Determining the model's scope of applicability
Regeneration quality	$\hat{\eta}_t$	$> 99.9\%$	Quality constraints
Data Communication	Status Frame	RTU-485	Uploaded parameters and downloaded setpoints

In order to show the nondominant relation between the volume and time of the liquid, the candidate solutions are shown in Figure 5, with the cycle time on the x axis, the regeneration liquid volume on the y axis, and the area of each point representing the power consumption. Then, the optimum solution is transferred to the power-consumption control algorithm with the measurement precision constraints.

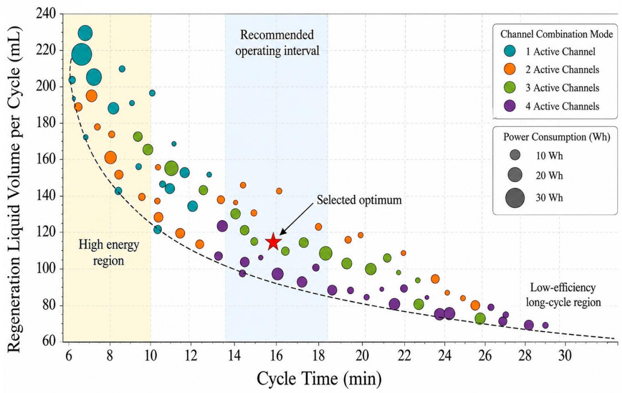

FIGURE 5. Scatter plot of multi-objective optimization for regenerated liquid usage versus cycle time.

D. ENERGY CONSUMPTION MINIMIZATION CONTROL ALGORITHM SUBJECT TO MEASUREMENT ACCURACY CONSTRAINTS

A combined approach of rolling prediction and constrained optimization is used in the energy consumption minimization control algorithm with measurement accuracy constraints, where the measurement errors of the conductivity sensors of hydrogen are used as hard constraints and the fluctuations of the power and control variables of the four regeneration channels are used as optimization variables[18]. During each sampling cycle, the controller reads the hydrogen conductivity, raw water conductivity, temperature, pressure, flow rate feedback, channel voltage and current, and sets the output regenerant dosage and cycle time set points; and, it uses a temperature compensation model and resin capacity status to predict what the hydrogen conductivity will be for the next sampling cycle. The algorithm should include: The parallel comparison error between the smart ion generator and a standard resin column should not exceed the range of plus or minus 3%, the removal efficiency of cations including NH_4^+ should be ≥99.9%, the voltage of regeneration should be 5 to 24V, the feedwater pressure should be below 0.25MPa, and when the water supply is interrupted, power outage occurs, communication is interrupted, and 4-20mA signal is out of range, control freeze should be implemented[19]. The single cycle control variable is determined by the following equation:

$$u_t^* = \arg\min_{u_t \in \Omega_t} \left[\alpha \sum_{k=1}^{4} U_{k,t} I_{k,t} + \beta (\hat{\kappa}_{t+1} - \kappa_t^{\text{ref}})^2 + \gamma \| u_t - u_{t-1} \|_2^2 \right]. \tag{12}$$

where u_t^* is the optimal control vector for cycle t, comprising the on/off states, output voltages, and operating frequencies of the four channels; Ω_t is the feasible region defined by measurement errors, ion removal rates, pressure, and equipment protection conditions; $U_{k,t}$ and $I_{k,t}$ are the voltages and currents of channels k, respectively; $\hat{\kappa}_{t+1}$ is the predicted hydrogen conductivity, and κ_t^{ref} is the current steady-state reference; u_{t-1} is the control vector from the previous cycle; α, β, and γ represent energy consumption, measurement error, and control smoothing weight, respectively. Only when precision constraints are satisfied will the embedded program rank a feasible solution and reduce the number of channel, frequency, or voltage; if the predicted error is close to the border, the measurement reliability is given priority, and the control command, the constraint margin, and the fault code are written to the operating database through RTU-485, providing a uniform data interface for the analysis of precision, power consumption, and dynamic response in subsequent experiments [20-21].

V. EXPERIMENTAL RESULTS AND ANALYSIS

A. EXPERIMENTAL PLATFORM, TEST SUBJECTS, AND PARAMETER SETTINGS

The experimental platform was installed at the steam-water sampling rooms and fine-treatment areas of Units 1 and 3 at Huayuan Power Plant. The experiment was done on 20 points of online measurement of hydrogen conductivity (10 points per unit). The steam-water sampling system included six data categories: condensate pump outlet, deaerator inlet, economizer inlet, reheated steam, start-up separator drain, and main steam. while the fine treatment system includes four data categories: total outlet and the outlets of mixed-bed columns A, B, and C. The trial operation period was from 15 December 2025 to 15 January 2026, with a feedwater pressure range of 0.15 to 0.20 MPa and feedwater specific conductivity of < 15 μS/cm. The data acquisition unit captures 20 channels of hydrogen conductivity, 4 status channels, pressure, temperature and regeneration voltage and current. 1–2 sets of measurement points are sampled each day and the sample points are connected in parallel with the smart ion generator and measured by the same portable conductivity meter as the resin column. The data was uploaded through RTU-485 which was used for data time synchronization, anomaly flagging and error calculations. The comparison threshold was determined as $\pm 3\%$ and this data was used for the following analysis of accuracy, energy consumption and operational stability.

B. COMPARISON OF RESIN EXCHANGE CAPACITY AND FAILURE CYCLES BEFORE AND AFTER DEEP REGENERATION

In order to compare the effects of normal regeneration and deep regeneration on the effective exchange capacity of the resin, the 20 measuring points were divided into 10 process placement categories, with each group comprising one measuring point from Unit 1 and Unit 3. Resin failure was defined as a reduction in capacity to 80 per cent of the original value. The results are presented in Table 3 and Table 4.

TABLE 3. Comparison of Effective Resin Exchange Capacity Before and After Deep Regeneration

Measurement Point Type	No. of Points	Before/(mmol·mL^{-1})	After/(mmol·mL^{-1})	Increment/(mmol·mL^{-1})	Increase, %
Coagulation Pump Outlet	2	0.96	1.48	0.52	54.17
Deaerator inlet	2	0.94	1.46	0.52	55.32
Economizer inlet	2	0.91	1.44	0.53	58.24
Left side of main steam	2	0.89	1.43	0.54	60.67
Right side of main steam	2	0.9	1.45	0.55	61.11
Reheated steam, left side	2	0.92	1.47	0.55	59.78
Reheated Steam (Right Side)	2	0.93	1.49	0.56	60.22
Filter No. 1 Outlet	2	1.05	1.56	0.51	48.57
Filter No. 2 Outlet	2	1.08	1.59	0.51	47.22
Filter No. 3 Outlet	2	1.1	1.61	0.51	46.36
Average	20	0.97	1.5	0.53	55.17

Based on the data in Table 3, it is seen that the average effective exchange capacity of the 20 measurement points after deep regeneration is 1.50 mmol·mL^{-1}, an increase of 0.53 mmol·mL^{-1} or 55.17%. Of these, the right side of the main steam line increased from 0.90 to 1.45 mmol·mL^{-1}, which is the most increase (61.11%) among the measurement locations; the left side of the main steam line and the right side of the reheat steam line increased by 60.67% and 60.22% respectively. The increase at the outlets of the Filters 1, 2 and 3, on the other hand, was 48.57%, 47.22% and 46.36%, respectively, and overall less than that at the steam-side measurement points. This difference reflects on important role of deep regeneration to restore resin exchange sites under high cation load to slow down reduction in resin's effective capacity of H-type resin and to provide capacity foundation for continuous hydrogen conductivity measurements.

TABLE 4. Comparison of Resin Failure Cycles and Maintenance Frequency Before and After Deep Regeneration

Monitoring Point Category	Before/d	After/d	Extension/d	Extension Factor	30-d Expected Maintenance Intervals
Condensate System	8.2	29.6	21.4	3.61	3.66→1.01
Water Supply System	7.6	28.8	21.2	3.79	3.95→1.04
Main Steam System	6.4	27.5	21.1	4.3	4.69→1.09
Reheated Steam System	6.8	28.1	21.3	4.13	4.41→1.07
Fine-tuning system	9.5	32.4	22.9	3.41	3.16→0.93
Average	7.7	29.3	21.6	3.81	3.97→1.03

The number of resin failure cycles before deep regeneration was determined by averaging the results of Table 4 resulting in 7.7 d. Following the application of continuous electrical regeneration, the equivalent failure cycle was extended to 29.3 d, which is 21.6 d more and is 3.81 times longer. The cycle was extended from 6.4 d to 27.5 d, an increase by a factor of 4.30 (maximum in the five categories of the main steam system); for the reheat steam system, the cycle was extended from 6.8 d to 28.1 d, an increase by a factor of 4.13. The fine treatment system showed the longest initial failure interval of 9.5 d and following deep regeneration, the interval was 32.4 d, which was the greatest absolute increase of 22.9 d. The average number of maintenance operations per measurement point, on a 30-day operating cycle, fell from 3.97 to 1.03, of which the fine treatment system was 0.93. This means that there is a need to replace the resin offline, switch to bypass and give the resin another chance to regenerate, which can be effectively avoided by continuous regeneration.

C. ANALYSIS OF ENERGY SAVINGS IN THE BOILER WATER HYDROGEN CONDUCTIVITY MEASUREMENT SYSTEM

In order to make it easier to compare the conventional resin tower with the deep regeneration system, the power consumption of the DC drive, the water supply, the wash bypass, the control and communication, and the maintenance support process was transformed into the accumulated electric energy in 30 days. The results are presented in Table 5.

Table 5 indicates that the total energy consumption at all the measurement points for 30 days reduced from 173.4 kWh to 112.5 kWh, which amounts to 60.9 kWh reduction or 35.12% reduction. The total average monthly energy use for each measurement point dropped from 8.67kWh/month to 5.63kWh/month. The energy consumption for resin regeneration, for regenerant recirculation was found to be reduced by 25.9 kWh and the energy consumption for online flushing and bypass operation was found to be reduced by 19.1 kWh. The combined effect of these two measures was 45.0 kWh which represented 73.89% of the total energy savings. This means that the main reasons for the energy savings are the elimination of offline acid regeneration, longer flushing and bypass switching, in favor of continuous electrical regeneration. Relatively limited potential for reduction was

TABLE 5. Comparison of Energy Consumption in the Reactor Water Hydrogen Conductivity Measurement System Before and After Deep Regeneration

Energy Consumption Component	Traditional/kWh	Deep/kWh	Change/kWh	Rate/%
Sample Water Conveyance and Pressure Stabilization	74.6	68.1	−6.5	−8.71
Resin Regeneration and Regeneration Solution Circulation	42.8	16.9	−25.9	−60.51
Online Flushing and Bypass Operation	31.5	12.4	−19.1	−60.63
Data Acquisition and Control Communications	5.8	7.2	1.4	24.14
Manual Maintenance Support Equipment	18.7	7.9	−10.8	−57.75
30-day total energy consumption	173.4	112.5	−60.9	−35.12

found for energy used for sample water transport since there is a need for continuous sampling and the reduction was only 8.71%. The energy consumption for data acquisition and communication of control actions rose from 5.8 kWh to 7.2 kWh, an increase of 1.4 kWh, but only 1.24% of the total energy consumption after optimization, which is significantly less than the energy savings described for the regeneration and maintenance phase. Manual maintenance support energy consumption has been reduced by 57.75% in line with the extended resin failure cycle and reduced maintenance frequency, thus providing an energy consumption basis for the subsequent analyses of measurement accuracy and operational reliability.

D. VERIFICATION OF MEASUREMENT ACCURACY, RESPONSE STABILITY, AND OPERATIONAL SAFETY

Parallel to the deep regeneration system, standard resin columns were tested to collect data on effective data rate, measurement error, response time, CV, and interlock action at 20 measuring points in 30 days. The results are presented in Table 6.

TABLE 6. Verification Results for Measurement Accuracy, Response Stability, and Operational Safety

Verification Metrics	Standard Resin Column System	Deep Regeneration System	Variation
Average Relative Error (%)	2.26	1.14	−1.12
Maximum Relative Error (%)	2.91	2.08	−0.83
90% response time (s)	182	76	−106
Steady-state coefficient of variation (%)	2.73	1.09	−1.64
24-hour zero drift/(μS·cm^{-1})	0.017	0.007	−0.010
Effective data rate/%	96.82	99.36	2.54
Fault Alarm Delay (s)	1.86	0.72	−1.14
Recovery time after protection/s	43.5	18.2	−25.3
Success rate of 36 protection tests/%	94.44	100	5.56

In Table 6, based on the results obtained, it can be seen that the average relative error of the deep regeneration system was reduced from 2.26% to 1.14% with the maximum error of 2.08%, all of which are below the ±3% limit for parallel comparison, the 90% response time was reduced by 106 s, the steady-state coefficient of variation was reduced from 2.73% to 1.09%, and the zero drift of 24 h was reduced by 0.010 μS/cm, which shows that continuous H^+ replenishment can reduce the hysteresis caused by resin failure and regeneration switching. The valid data rate rose to 99.36% and the rate of invalid data in 30 days reduced from 3.18% to 0.64%. The deep regeneration system was able to trigger an output shutdown and alarms in all 36 tests, 12 for each test condition of water supply interruption, power outage and overpressure. The alarm delay was 0.72 s and the recovery time was 18.2 s, which are 1.14 s and 25.3 s less than the standard system, respectively. In order to differentiate the fluctuation distributions of the various measurement points and operating periods further, Figure 6 is plotted using the coefficient of variation of hydrogen conductivity as color scale.

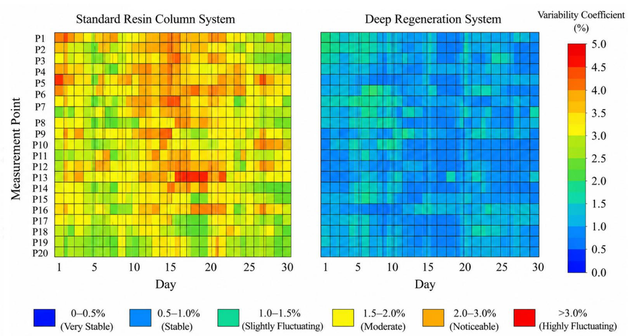

FIGURE 6. Heatmap of hydrogen conductivity response stability across 20 measurement points during a 30-day operating cycle.

E. ABLATION EXPERIMENTS AND CONTRIBUTION ANALYSIS OF KEY ALGORITHMS FOR ENERGY-SAVING CONTROL

Single module was removed under the same measurement point, load conditions and operating cycle and with other parameters unchanged in order to determine the independent functions of the four kinds of algorithms: Resin Capacity Decay Detection, Hydrogen Conductivity Trend Determination, Regeneration Liquid Volume-Circulation Time Optimization, and Energy Consumption Control under accuracy constraints. This is displayed in Table 7.

TABLE 7. Results of Ablation Experiments for Key Energy-Saving Control Algorithms

Algorithm Configuration	Energy/30 d (kWh)	Reduction/%	Average Error/%	90% Response (s)	Effective Data/%
Complete Algorithm	112.5	35.12	1.14	76	99.36
Identification of Capacity Decay	122.3	29.47	1.46	91	98.77
Trend removal	127.1	26.7	1.39	104	98.92
Optimization of Stripping Volume vs. Time	130.6	24.68	1.22	82	99.18
Control without accuracy constraints	125.2	27.8	2.31	73	–

From table 7 it can be concluded that the total energy consumption of the complete algorithm is 112.5 kWh for

30 days. With the elimination of the liquid volume–time optimization, the energy consumption became 130.6 kWh (an increase of 18.1 kWh) and the energy savings rate became 24.68% (from 35.12%). This means that optimizing the combination of the regeneration cycle and the amount of liquid circulated is the critical one to minimize ineffective operation during electrical regeneration. With the removal of the hydrogen conductivity trend assessment, the energy consumption rose by 14.6 kWh, and the 90% response time went up from 76 s to 104 s, which means that fixed-cycle regeneration is prone to cause premature or delayed activation. With the removal of the accuracy constraint control, the response time was reduced to 73 s, while the average relative error is increased to 2.31% and the effective data rate is reduced to 97.86%, meaning that co-optimization of only low energy consumption and fast response time can lead to a decrease of the accuracy margin. Capacity decay identification removed, energy consumption was increased by 9.8 kWh and the average error of 1.46% showed that capacity state estimation can help to reduce overcompensation due to the decrease of resin performance. Figure 7 presents the ranking of the marginal contributions of the liquid volume–time optimization, trend determination, accuracy constraint control and capacity decay identification when the energy consumption increments of each eliminated item are normalized with respect to the complete algorithm.

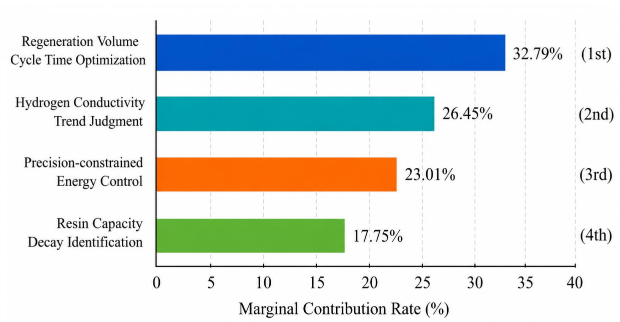

FIGURE 7. Ranking of Marginal Contribution Rates for Key Energy-Saving Control Algorithms.

VI. CONCLUSIONS

The deep regeneration technology combines ionization-based hydrogen generation, online resin reset, four-channel coordinated control, and measurement accuracy limit into one control system to solve the problems of frequent offline regeneration of traditional resin columns, long bypass flushing time and difficult to control dispersed energy consumption. Meanwhile, the average effective exchange capacity of the resin rose from 0.97 to 1.50 mmol·mL^{-1}, the failure cycle extended from 7.7 to 29.3 d, while the total energy consumption in 30 d fell from 173.4 to 112.5 kWh, which decreased by 35.12%, and the average relative error decreased to 1.14%, and the average effective steam and water quality monitoring rate was improved to 99.36%, which shows that the water and steam quality monitoring has not been affected by the energy-saving optimization. The innovative value is mainly focused on the combination of the following techniques: Resin capacity decay identification, hydrogen conductivity trend triggering, liquid volume–time coordinated optimization, and accuracy-constrained energy consumption control. The application is still limited by the test cycle, the number of measurement points and types of power plant operating conditions, and the influence of complex start-up and shutdown processes, abnormal water quality impacts and long-term membrane fouling is still to be monitored. Future research may involve more validation in multiple units and different water quality conditions, more self-calibration of mass transfer parameters and lifetime prediction model, and more effort to evolve the system of measuring conductivity to achieve low-maintenance, high stability and adaptive energy saving.

REFERENCES

[1] J. Godifredo, L. Ruiz, S. Hernández, et al., "Recovering nitrogen from anaerobic membrane bioreactor permeate using a natural zeolite ion exchange column," *Water*, vol. 16, no. 19, p. 2820, 2024, doi: 10.3390/w16192820.

[2] S. Y. Yeoh, K. W. Lai, S. Y. Pung, et al., "Optimising brine regeneration of ion-exchange resins: Effects of pre-treatment temperature, brine concentration, and ratio," *Clean Technologies and Environmental Policy*, vol. 28, no. 3, p. 62, 2026, doi: 10.1007/s10098-025-03367-7.

[3] N. M. Marin, M. Nita Lazar, M. Popa, et al., "Current trends in development and use of polymeric ion-exchange resins in wastewater treatment," *Materials*, vol. 17, no. 23, p. 5994, 2024, doi: 10.3390/ma17235994.

[4] J. Wullenweber, J. Bennert, T. Mantel, et al., "Characterizing macroporous ion exchange membrane adsorbers for natural organic matter (NOM) removal—adsorption and regeneration behavior," *Membranes*, vol. 14, no. 6, p. 124, 2024, doi: 10.3390/membranes14060124.

[5] M. Bernardi, A. L. Hantson, G. Caulier, et al., "Ni^{2+} removal by ion exchange resins and activated carbon: A benchtop NMR study," *International Journal of Environmental Science and Technology*, vol. 21, no. 13, pp. 8337–8360, 2024, doi: 10.1007/s13762-024-05547-2.

[6] A. Mohammed, C. Mohammed, A. Mautner, et al., "On the performance of Sargassum-derived calcium alginate ion exchange resins for Pb^{2+} adsorption: Batch and packed bed applications," *Environmental Science and Pollution Research*, vol. 31, no. 21, pp. 31224–31239, 2024, doi: 10.1007/s11356-024-33314-w.

[7] E. Apraku, C. M. Laguna, R. M. Wood, et al., "Enhancing resource recovery through electro-assisted regeneration of an ammonia-selective cation exchange resin," *ACS ES&T Water*, vol. 4, no. 10, pp. 4521–4532, 2024, doi: 10.1021/acsestwater.4c00543.

[8] Y. Rasouli, B. Barbeau, R. Maltais-Tariant, et al., "Impact of cleaning on membrane performance during surface water treatment: A hybrid process with biological ion exchange and gravity-driven membranes," *Membranes*, vol. 14, no. 2, p. 33, 2024, doi: 10.3390/membranes14020033.

[9] C. Graham, C. Kassar, and T. H. Boyer, "Alcohol regeneration of anion exchange resin loaded with per- and polyfluoroalkyl substances and organic contaminants," *AWWA Water Science*, vol. 6, no. 4, p. e1380, 2024, doi: 10.1002/aws2.1380.

[10] K. Zimmermann, P. Sampara, R. Ziels, et al., "Biological contributions to biological ion exchange," *Environmental Science: Water Research & Technology*, vol. 10, no. 4, pp. 877–888, 2024, doi: 10.1039/d3ew00766a.

[11] M. F. Ahmer and M. K. Uddin, "Structure properties and industrial applications of anion exchange resins for the removal of electroactive nitrate ions from contaminated water," *RSC Advances*, vol. 14, no. 45, pp. 33629–33648, 2024, doi: 10.1039/d4ra03871a.

[12] H. Asim, H. Zeidan, and M. E. Marti, "Effective isolation of succinic acid from aqueous media with the use of anion exchange resins," *RSC Advances*, vol. 14, no. 24, pp. 16765–16777, 2024, doi: 10.1039/d4ra02110j.

[13] A. El-Tantawy, E. M. Abu Elgoud, and S. E. A. Sharaf El-Deen, "Evaluation of anion exchange resin for sorption of selenium (IV) from aqueous solutions," *BMC Chemistry*, vol. 19, no. 1, p. 10, 2025, doi: 10.1186/s13065-024-01356-3.

[14] A. L. Mungan, E. A. Hjelvik, A. P. Straub, et al., "A hybrid anion exchanger with nanoscale zero valent iron for trace hexavalent chromium removal from drinking water," *Environmental Science: Advances*, vol. 3, no. 11, pp. 1598–1615, 2024, doi: 10.1039/d4va00246f.

[15] K. Chruszcz-Lipska and E. Szostak, "A study of the structure of an anion exchange resin with a quaternary ammonium functional group by using infrared spectroscopy and DFT calculations," *Materials*, vol. 17, no. 24, p. 6132, 2024, doi: 10.3390/ma17246132.

[16] S. Bergamasco, L. A. Hein, L. Silvestri, et al., "Innovative Nafion- and lignin-based cation exchange materials against standard resins for the removal of heavy metals during water treatment," *Separations*, vol. 11, no. 12, p. 357, 2024, doi: 10.3390/separations11120357.

[17] F. Galluccio, A. Santi, E. Rizzi, et al., "An integrated strategy for pre-disposal of spent cation-exchange resins by repurposing industrial by-products," *Sustainability*, vol. 17, no. 18, p. 8241, 2025, doi: 10.3390/su17188241.

[18] V. Romanovski and V. Gruzinova, "Aggregate from spent ion-exchange resins for petroleum products removal from wastewater," *Waste and Biomass Valorization*, vol. 17, no. 2, pp. 857–865, 2026, doi: 10.1007/s12649-025-03158-7.

[19] A. L. Ling, T. Stegner, M. Thompson, et al., "Spent media management pathways for PFAS treatment applications," *Water Environment Research*, vol. 97, no. 7, p. e70130, 2025, doi: 10.1002/wer.70130.

[20] W. H. DiGuiseppi, C. J. Newell, G. Carey, et al., "Available and emerging liquid treatment technologies for PFASs," *Remediation Journal*, vol. 34, no. 3, p. e21782, 2024, doi: 10.1002/rem.21782.

[21] A. Q. Jasim and S. K. Ajjam, "Removal of heavy metal ions from wastewater using ion exchange resin in a batch process with kinetic isotherm," *South African Journal of Chemical Engineering*, vol. 49, no. 1, pp. 43–54, 2024, doi: 10.1016/j.sajce.2024.04.002.